$$\tau_D = \frac{w^2}{4D} \qquad (6)$$

where w is radial length of the confocal volume element. With the assumption that the studied species are spherical (which we confirmed using TEM or *in situ* AFM), the hydrodynamic radius R_h can be obtained from the Stokes-Einstein equation:

$$D = \frac{kT}{6\pi\eta R_h} \qquad (7)$$

where η is the solvent viscosity, k is Boltzmann's constant, and T is the absolute temperature. In the case of spherical structures, the mass M is proportional to R_h^3. Therefore, if a reference molecule with a known mass is measured, M of the studied species can be obtained as follows:

$$M = \left(\frac{\tau_D}{\tau_{D\,\mathrm{Reference}}}\right)^3 M_{\mathrm{Reference}} \qquad (8)$$

In the case of non-spherical structures, by measuring a reference with known diffusion coefficient $D_{\mathrm{Reference}}$, D of the studied species is obtained as follows:

$$D = \left(\frac{\tau_{D\,\mathrm{Reference}}}{\tau_D}\right) D_{\mathrm{Reference}} \qquad (9)$$

The relative abundance of each assembly was obtained by integrating each i-th peak of $P(\tau_D)$.

In Figs. 1*B*, 2*C*, 3*B*, and 3*C*, the distribution of assembly mass (log scale) or diffusion coefficient (log scale) is shown. To show the distribution in the graphs with the logarithmic scale on the abscissa, we newly introduced two parameters, $\tilde{M}$ (=log M) and $\tilde{D}$ (=log D) and transformed $P(\tau_D)$ either into $\tilde{P}(\tilde{M})$ (the distribution function of $\tilde{M}$) or $\overline{P}(\tilde{D})$ (the distribution function of $\tilde{D}$), where $\tilde{P}(\tilde{M})$ and $\overline{P}(\tilde{D})$ satisfy the following normalization conditions,

$$\int_0^\infty \tilde{P}(\tilde{M})d\tilde{M} = 1 \qquad (10)$$

$$\int_0^\infty \overline{P}(\tilde{D})d\tilde{D} = 1 \qquad (11)$$

These transformations are performed according to the following equations,

$$\tilde{P}(\tilde{M}) = \frac{1}{3}P(\tau_D)\tau_D \log_e 10 \qquad (12)$$

$$\overline{P}(\tilde{D}) = -P(\tau_D)\tau_D \log_e 10 \qquad (13)$$

$\tilde{P}(\tilde{M})$ (Figs. 1*B*, 2C, 3B&C) or $\overline{P}(\tilde{D})$ (Supplemental Fig. S7) is shown in the graphs.

In FCS measurements, the contribution of each component to the correlation curve is related to both relative abundance and relative brightness (10). If all components have equal brightness, the relative abundance of each assembly can be obtained by integrating each i-th peak of $P(\tau_D)$. This is true for ASPDs and early fibril intermediates, but not for fibrils containing more than one fluorophore. In the latter case, a rough estimate of the apparent relative abundance of the fibrils was obtained by integrating the i-th peak of $P(\tau_D)$(for details, see "*In situ monitoring of fibril formation*"). To confirm the rough estimates thus obtained, mature fibrils were separated in the retentate fractions of 0.1-μm filters (confirmed using TEM) and their amount was directly obtained from the fluorescence count using a fluorometer (Twinkle LB970; Berthold Technologies GmbH).

Analysis of FCS data obtained from immunoprecipitation eluates- As described above, the immunoisolated ASPDs were measured in highly viscid Gentle Elution Buffer (GEB; Pierce). As shown below, although the GEB itself does not contain fluorescent components, noisy signals were observed in a

very fast diffusion time range ($\tau < 0.01$ ms) of $G_{exp}(\tau)$ with samples in the GEB (either Alexa Fluor 532 or ASPDs). Such noisy signals were absent in $G_{exp}(\tau)$ with samples in 0.5X PBS. Although we do not know why the signal in the fast time range of $G_{exp}(\tau)$ was noisy, we believe that quenching of the fluorescence of the Alexa Fluor 532 dye in the GEB could lead to an increase in background noise, causing noisy signals at very fast diffusion time, because we found that the count per molecule of Alexa Fluor 532 in the GEB was about a tenth lower than that of Alexa Fluor 532 in 0.5X PBS. Because these noisy signals were indistinguishable from triplet signals, we only analyzed $G_{exp}(\tau)$ in a slow diffusion time range ($\tau > 1.0$ ms) for the immunoisolated ASPDs (the diffusion time of Alexa Fluor 532 dye in the GEB was ~0.43 ms). In this time range, the effect of the triplets was negligible; thus, the following equation of the original triplet-free model was used (11).

$$G_{exp}(\tau)_{GEB} = 1 + A\int_0^\infty \frac{1}{\left(1+\frac{\tau}{\tau_D}\right)\sqrt{\left(1+\frac{\tau}{s^2\tau_D}\right)}} P(\tau_D)\, d\tau_D \qquad (14)$$

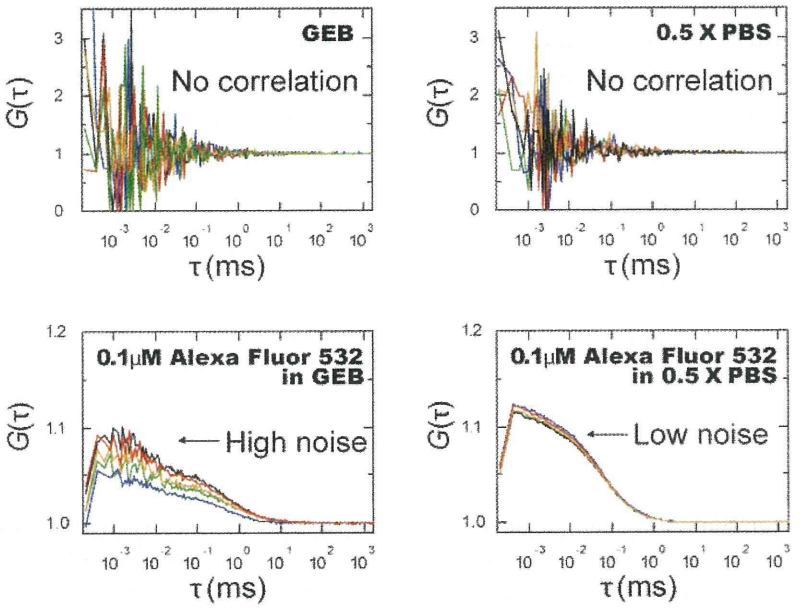

Toxicity assays- The Animal Care and Experimentation Committee of Mitsubishi Kagaku Institute of Life Sciences and Kyoto University approved all animal experiments. Primary cultures from rat septum regions, which include septal and basal forebrain cholinergic neurons, were prepared as described (1) and plated at a density of 2.4 x 10^5 cells/cm^2 on a poly-L-lysine (0.01%; Nacalai Tesque 28360-14)-coated 48-well plastic plates (0.3 ml/well). After 50-55 hrs, the medium was replaced with a serum-free neurobasal media containing B27 supplements, 0.5 mM L-glutamine, and 50 μg/ml gentamicin. After an additional 5 days of culture, the cells were treated with ASPD samples. Primary rat hippocampal cultures

were prepared (4) and plated at a density of 3.6 x 10^4 cells/cm^2 (48-well plastic plates) on a polyethyleneimine (0.02% PEI; Sigma P3143)-coated wells in neurobasal media containing B27 supplements and 2.5 μM L-glutamine. Cultures were maintained in this medium for a week. Then, approximately half of the medium was replaced once a week with neurobasal media containing B27 supplements, 2.0 μM L-glutamine, and 10% (v/v) astrocyte-derived conditioned medium (Sumitomo Bakelite Co., Ltd. MB-X9501). For the toxicity evaluation, apoptosis was determined quantitatively by monitoring cytoplasmic histone-associated DNA fragments with sandwich ELISA (Cell Death Detection ELISAplus, Roche Diagnostics), according to the manufacturer's instructions. The cells were treated with ASPD samples at 19-20 *days in vitro*. The apoptotic activity was expressed as absorbance difference (A_{405}-A_{450}) normalized by the amount of Aβ present. Alternatively, toxicity was also estimated by monitoring lactate dehydrogenase (LDH) activity in the culture supernate, which reflects plasma membrane damage, using Cytotoxicity Detection Kitplus (Roche Diagnostics) essentially according to the manufacturer's instructions. The toxicity was expressed as absorbance difference (A_{490}-A_{655}) normalized by the amount of Aβ present.

Statistics- The statistical significance of the differences among groups was determined by applying Games-Howell or Scheffé *post hoc* tests using StatView® 5.0 (SAS Institute Inc., Cary, NC, USA).

Table S1. Characteristics of ASD Antibodies and Anti-pan Aβ Antibodies

Antibody	Preference among Aβ types in dot blotting	K_d for ASPDs (nM)	Epitope map	Response to APP in dot blotting	Response to fibrils in immuno-TEM	Blockade of ASPD toxicity
rpASD1	ASPD	0.005	Several regions[a]	-	-	+
haASD1	ASPD	0.0005	Could not be determined[b]	-	-	-
6E10	All types	0.2	Aβ5-9[c]	+	+	-
82E1	All types	nd	Aβ1-5[c]	-	*nd*	-

nd; not determined.

The characteristics of ASPD-specific antibodies (upper two rows) used in this work and commercially available anti-pan Aβ antibodies (lower two rows) are summarized. The original data are from our previous report (2). [a]The binding of rpASD1 to synthetic-ASPDs was most strongly inhibited by N-terminal pentapeptides of Aβ. In addition, the binding was also inhibited by specific sets of non-N-terminal pentapeptides. The data suggest that different Aβ regions exist in close proximity to form the ASPD-specific epitope. [b]The binding of haASD1 to synthetic-ASPDs was not inhibited by the addition of any pentapeptide, suggesting that haASD1 recognizes a non-linear epitope formed by non-contiguous Aβ regions. [c]For 6E10 and 82E1, which did not discriminate ASPDs from other types of Aβ, complete inhibition was attained with a single pentapeptide in each case.

Fig. S1 Matsumura et al.

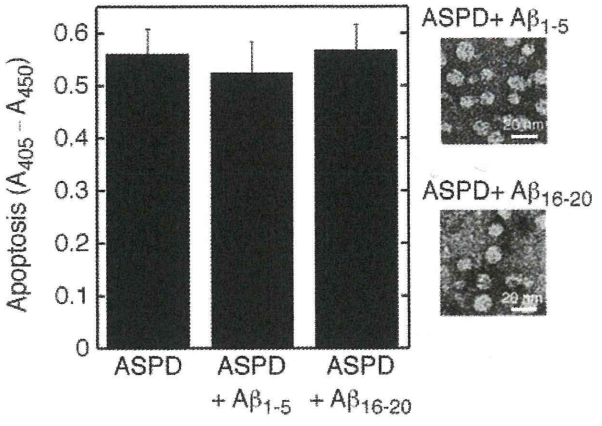

Supplemental Fig. S1. Excess amounts of $A\beta_{1-5}$ (DAEFR) or $A\beta_{16-20}$ (KLVFF) did not block toxic ASPD formation. ASPDs were prepared *in vitro* from 50 μM solutions of $A\beta_{1-42}$ using the slow rotation method (1) with or without a 10-fold molar excess of $A\beta_{1-5}$ or $A\beta_{16-20}$. Apoptotic activity against rat primary septal neuronal cultures was determined quantitatively by monitoring DNA fragmentation (n=18; see Additional Experimental Procedures). We also confirmed the presence of ASPDs using TEM (right panels). Neither $A\beta_{1-5}$ nor $A\beta_{16-20}$ affected the formation of toxic ASPDs.

Fig. S2 Matsumura et al.

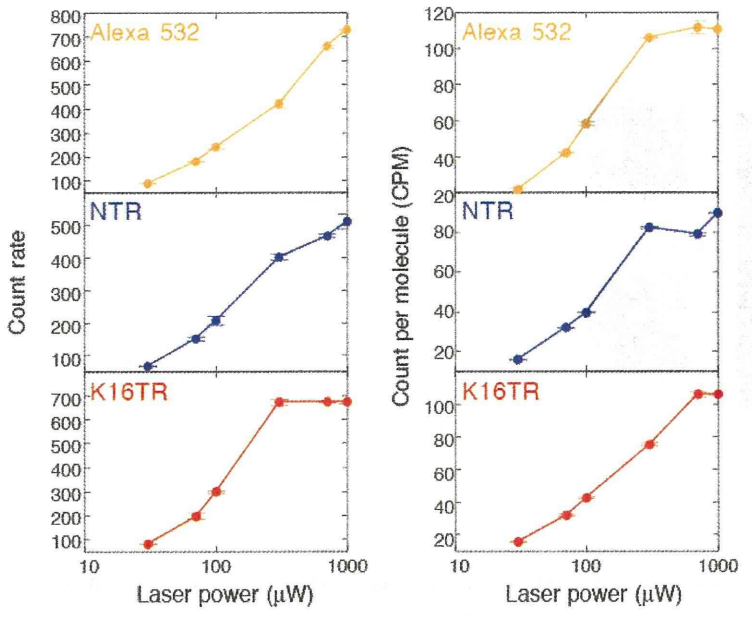

Supplemental Fig. S2. Optimization of laser power (intensity) for fluorescent probes. Since too strong a laser power saturates fluorescence absorption, while too weak a laser power results in a low signal-to-background ratio, NTR and K16TR (freshly dissolved at 0.05 μM in 0.5X PBS) were examined using FCS at various laser intensities. Between 30 and 300 μW, both the average photon number/sec (the count rate) and the count rate/ number of fluorescent molecules in a confocal volume (the count per molecule) increased with increasing laser power (n = 5). Therefore, we routinely set the laser power at 100 μW, which gave a high signal-to-background ratio (>100:1).

Fig. S3 Matsumura et al.

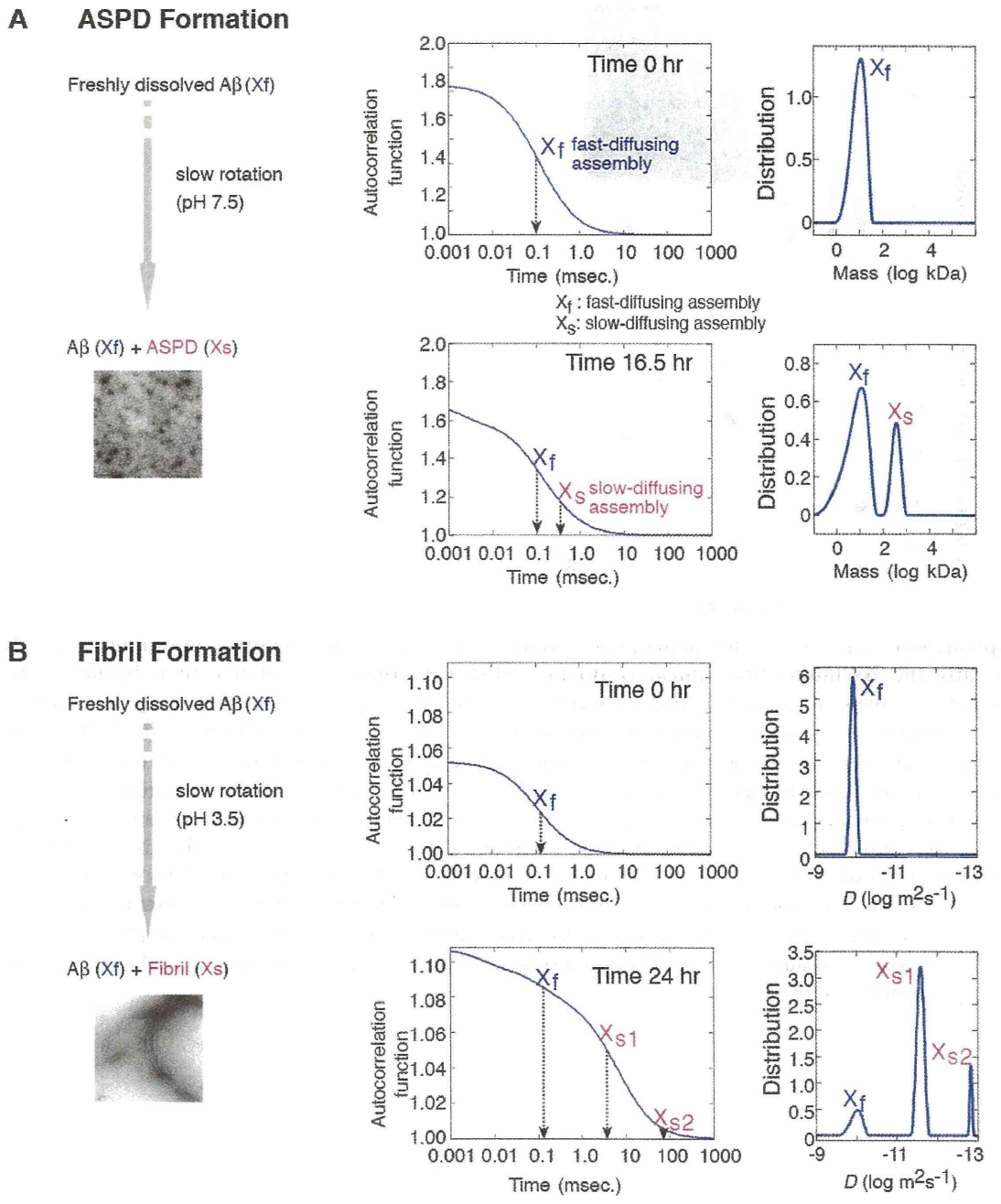

Supplemental Fig. S3. Evaluation of Aβ assembly processes into ASPDs or fibrils using TEM and FCS analyses. Analyses of ASPD formation (*A*) and fibril formation (*B*) (details in Experimental Procederes). Fibril formation is shown in apparent mass in Fig. 3 and in *D* in Fig. S7.

Fig. S4 Matsumura et al.

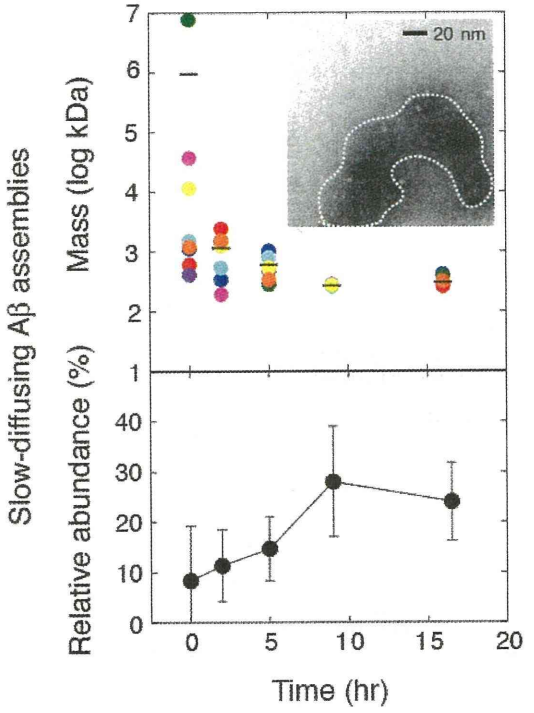

Supplemental Fig. S4. Time-dependent changes in mass and relative abundance of the slow-diffusing assemblies that appeared during ASPD formation. Each colored dot in the upper panel represents the mass of the slow-diffusing assemblies detected at the indicated time during the course of ASPD formation in a series of independent experiments (n = 8), and each bar represents the average mass at the indicated time. The average relative abundance of these assemblies is shown in the lower panel. Aβ trimers were the dominant species during the first 2 hrs of slow rotation. However, small amounts of slow-diffusing species with variable mass and relative abundance were detected reproducibly at these time points. Cloud-like uranyl acetate-stained structures (dotted line in *Inset*), clearly distinct from the staining of buffer-derived salts, were observed in low levels by TEM during the first 2 hrs of slow rotation, and we speculate that these species might be metastable and be destroyed during the sample preparation for TEM. It is unlikely that all of these species represent insufficiently dissolved Aβ (amorphous structure in Fig. 1B, arrow) because at 2 hrs, such amorphous structures were decreased in TEM, while these species were increased in FCS.

Fig. S5 Matsumura et al.

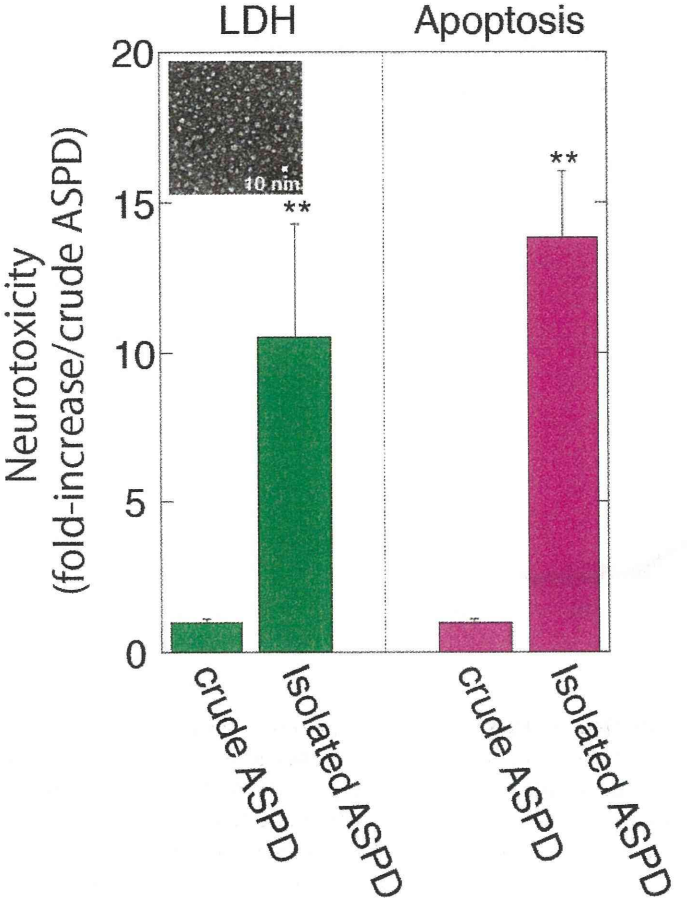

Supplemental Fig. S5. Neurotoxicity of the purified ASPDs. Neurotoxicity of the most toxic ASPDs immunoisolated by anti-ASPD haASD1 antibody was compared with that of crude ASPDs either by LDH release assay (monitoring plasma membrane damage) or by apoptotic activity assay (monitoring DNA fragmentation) according to the manufacturer's instructions using hippocampal rat primary neuronal cultures at 19 days *in vitro*. Specific activities of the isolated ASPDs are shown as fold-increase against those of the crude ASPDs (mean ± SD; Scheffé *post-hoc* test, **, $p < 0.001$, $n > 4$). The TEM image of the isolated ASPDs is shown in the inset.

Fig. S6 Matsumura et al.

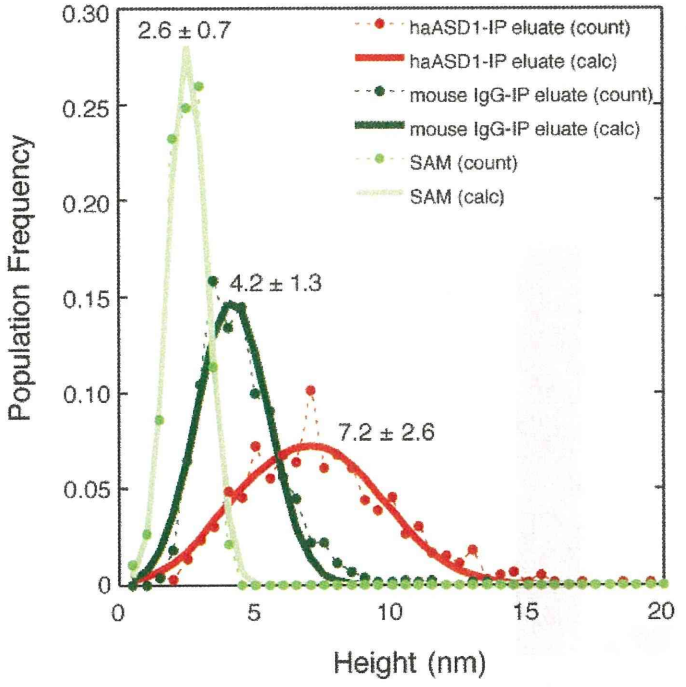

Supplemental Fig. S6. The size of the purified ASPDs. We have previously shown that ASPDs are spheres that have a diameter equal to their height (1) using *in situ* AFM in solution. We therefore determined the size of the purified ASPDs by measuring their height using *in situ* AFM. We examined the height of each structure in anti-ASPD haASD1-immunoprecipitation (IP) eluate (haASD1-IP eluate; n = 591), normal mouse IgG-IP eluate (mouse IgG-IP eluate; n = 759), and self-assembled monolayers (SAMs) on which samples were deposited (SAM; n = 185). Above, the population frequency of the measured height is shown as "count" and that of the fitted data is shown as "calc.". On SAMs, some structures of 2.6 ± 0.7 nm in height were detected. In mouse IgG-IP eluates, ASPD-sized structures were absent, but smaller structures of 4.2 ± 1.3 nm in height were present. These smaller structures were considered to be derived from blocking reagents contained in the elution buffer (Additional Experimental Procedures), since ASPDs and other Aβs were hardly detectable in dot blots using anti-ASPD antibodies (Fig. 2B) or anti-pan Aβ antibodies (2). In contrast, haASD1-IP eluates contained mostly (~94%) spherical structures of 7.2 ± 2.6 nm in height. FCS analysis revealed that the average mass of the unpurified ASPD preparations was 330 ± 58 kDa, while that of the immunoisolated ASPDs was 128 ± 44 kDa. Consistently with this, *in situ* AFM showed that the average height of the unpurified ASPDs was 9.1 ± 2.0 nm (1), while that of the immunoisolated ASPDs was 7.2 ± 2.6 nm.

Fig. S7 Matsumura et al.

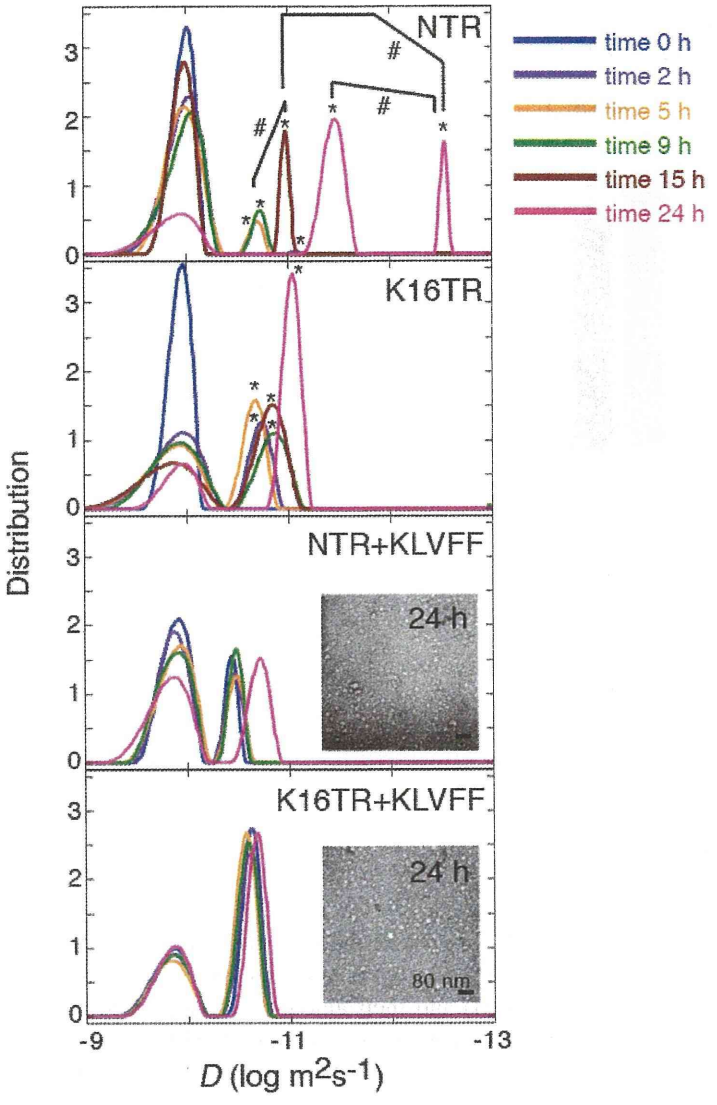

Supplemental Fig. S7. Time course of fibril formation. Fibrils were formed from 100 μM solutions of $A\beta_{1\text{-}40}$ with 0.1 μM NTR or K16TR at pH 3.5. At the onset of fibril formation, a 10-fold molar excess of $A\beta_{16\text{-}20}$ (KLVFF) was added to the $A\beta_{1\text{-}40}$ solutions, and analyses using TEM (*Inset*) and FCS were performed as in Fig. 3 (*, $p < 0.005$ by Scheffé *post-hoc* test compared with the fast-diffusing assembly corresponding to dimers; #, $p < 0.005$ by Scheffé *post-hoc* test). The normalized distribution of assembly diffusion coefficient is shown, as in Fig. 1B.

Fig. S8 Matsumura et al.

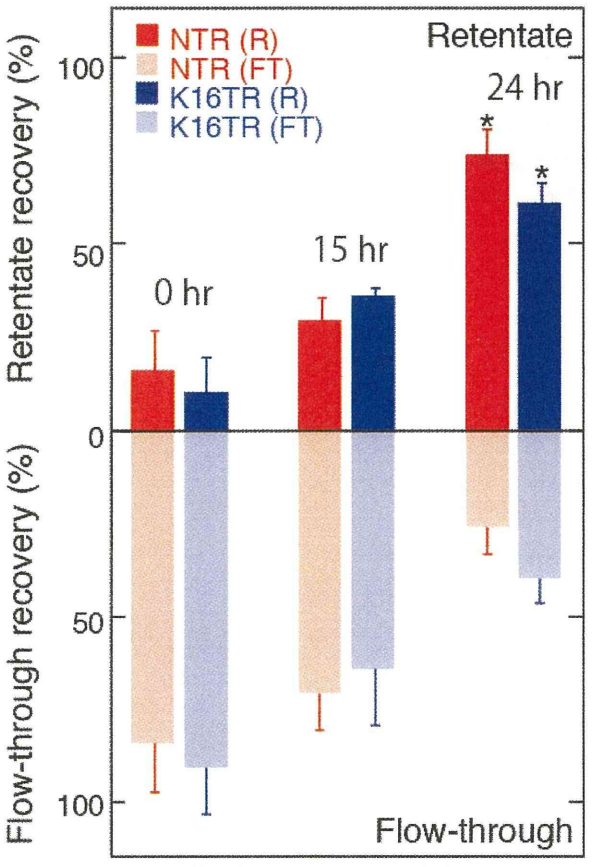

Supplemental Fig. S8. Estimation of fibril amount. We used a probe ratio of 1/1000 for fibrils. To confirm rough estimates calculated from FCS data (see Fig. 3), mature fibrils were separated in the retentate fractions of 0.10-μm filters (confirmed using TEM) and their amount was calculated from the fluorescence count using a fluorometer (Twinkle LB970; Berthold Technologies GmbH; n=5)(mean ± SD; *, $p < 0.005$ by Scheffé *post-hoc* test, n = 6), which was also confirmed by quantitative amino acid analysis (1).

Supplemental References

1. Hoshi, M., Sato, M., Matsumoto, S., Noguchi, A., Yasutake, K., Yoshida, N., and Sato, K. (2003) *Proc. Natl. Acad. Sci. U.S.A.* **100**, 6370-6375
2. Noguchi, A., Matsumura, S., Dezawa, M., Tada, M., Yanazawa, M., Ito, A., Akioka, M., Kikuchi, S., Sato, M., Ideno, S., Noda, M., Fukunari, A., Muramatsu, S., Itokazu, Y., Sato, K., Takahashi, H., Teplow, D. B., Nabeshima, Y., Kakita, A., Imahori, K., and Hoshi, M. (2009) *J. Biol. Chem.* **284**, 32895-32905
3. Wang, H., Chen, S., Li, L., and Jiang, S. (2005) *Langmuir* **21**, 2633-2636
4. Bayburt, T. H., and Sligar, S. G. (2002) *Proc. Natl. Acad. Sci. U.S.A.* **99**, 6725-6730
5. Provencher, S. W. (1982) *Comput. Phys. Commun.* **27**, 213-227
6. Provencher, S. W. (1982) *Comput. Phys. Commun.* **27**, 229-242
7. Widengren, J., Mets, Ü., and Rigler, R. (1995) *J. Phys. Chem.* **99**, 13368-13379
8. Eggeling, C., Widengren, J., Rigler, R., and Seidel, C. A. M. (1998) *Anal. Chem.* **70**, 2651-2659
9. Asimov, M. M., Gavrilenko, V. N., and Rubinov, A. N. (1990) *J. Lumin.* **46**, 243-249
10. Palmer, III, A. G., and Thompson, N. L. (1987) *Biophys. J.* **52**, 257-270
11. Aragón, S. R., and Pecora, R. (1976) *J. Chem. Phys.* **64**, 1791-1803

Chemical Science

View Online
Dynamic Article Links

Cite this: DOI: 10.1039/c1sc00071c

www.rsc.org/chemicalscience

EDGE ARTICLE

^{19}F MRI detection of β-galactosidase activity for imaging of gene expression†

Shin Mizukami,[ab] Hisashi Matsushita,[a] Rika Takikawa,[a] Fuminori Sugihara,[c] Masahiro Shirakawa[d] and Kazuya Kikuchi*[ab]

Received 3rd February 2011, Accepted 23rd March 2011
DOI: 10.1039/c1sc00071c

Imaging of gene expression by magnetic resonance imaging (MRI) yields direct information regarding living systems that cannot be obtained *via* other methods. In this study, we report the rational design and synthesis of a novel ^{19}F MRI probe that detects β-galactosidase (β-gal) activity, enabling the imaging of gene expression in cells. The ^{19}F MRI signal of the probe was quenched by the intramolecular paramagnetic resonance enhancement from a Gd^{3+} ion. A contrivance was made in the probe structure to recover the ^{19}F MRI signal after hydrolysis by β-gal with a following self-immolative reaction. This ^{19}F MRI signal change was observed in the physiological aqueous condition. The probe could also detect β-gal activity in fixed HEK293T cells. In conclusion, this new probe enables the ^{19}F MRI detection of cellular gene expression. The probe design strategy is also expected to lead to the development of MRI probes for a wide variety of hydrolase activities.

Introduction

Imaging of gene expression gives us various information such as the expression timing of target proteins, gene transfer efficiency, and detection of a disease-related gene expression. To monitor gene expression by various methods, reporter proteins[1–3] are useful. Fluorescence detection of gene expression by using fluorescent proteins is particularly important because fluorescence measurement has several advantages including sensitivity, convenience, spatiotemporal resolution, *etc.* However, the poor transmission of fluorescence is one of the limitations for the *in vivo* application. Use of magnetic resonance imaging (MRI)[4] is one way to solve the problem, because MRI yields high-resolution images of deep regions of living animal bodies. Therefore, MRI is currently considered to be one of the most promising techniques for *in vivo* investigation of physiological events.[5]

Recently, several smart ^{1}H MRI probes for visualizing gene expression *via* β-galactosidase activity have been reported.[6] In principle, however, such ^{1}H MRI signal enhancement needs to be discriminated from the background ^{1}H MRI signals of water, fatty acids, and other biomolecules. To avoid this limitation, we have focused on the use of ^{19}F MRI. ^{19}F, as well as ^{1}H, is one of the most highly sensitive nuclei for NMR spectroscopy and MRI,[7] and almost no intrinsic ^{19}F MRI signals are observed in animal bodies. Thus, ^{19}F MRI probes that can visualize biological events have been increasingly reported.[8] We have also developed off-on switching ^{19}F MRI probes to detect protease activity[9] on the basis of paramagnetic relaxation enhancement (PRE),[10] a phenomenon in which the relaxation of nuclei is enhanced near paramagnetic molecules.

By expanding this probe principle, we here report a novel ^{19}F MRI probe that detects cellular gene expression. β-galactosidase (β-gal) was chosen as the reporter protein for gene expression, because it has several advantages where reporter proteins are concerned.[3,11] The advantages are as follows: (1) induction of β-gal synthesis occurs over a large dynamic range, (2) β-gal is tolerated and functional in many organisms including mammals, (3) various substrates of β-gal are available or easily synthesized, (4) many assay methods that use β-D-galactopyranoside-coupled aglycones are available, and (5) there is almost no intrinsic β-gal activity in mammalian cells. Therefore, β-gal is one of the most widely used reporter proteins for imaging of gene expression. Through the detection of β-gal activity, we tried ^{19}F MRI detection of cellular gene expression.

Results

Probe design concept, synthesis and physical properties

Several probes have been developed that can detect β-gal activity.[3,12] X-gal is one of the most widely used probes among them. Such β-D-galactopyranoside-coupled aromatic compounds are known to be the substrates of β-gal, and several fluorescent probes for β-gal have been developed. Taking this substrate

[a]*Division of Advanced Science and Biotechnology, Graduate School of Engineering, Osaka University, 2-1 Yamadaoka, Suita, Osaka, 565-0871, Japan. E-mail: kkikuchi@mls.eng.osaka-u.ac.jp; Fax: (+81) 6-6879-7875*
[b]*Immunology Frontier Research Center (IFReC), Osaka University, Osaka, 565-0871, Japan*
[c]*International Graduate School of Arts and Sciences, Yokohama City University, Kanagawa, 230-0045, Japan*
[d]*Graduate School of Engineering, Kyoto University, Kyoto, 615-8510, Japan*
† Electronic supplementary information (ESI) available: Synthesis of compounds, representative HPLC chromatograms and ^{19}F NMR. See DOI: 10.1039/c1sc00071c

recognition property of β-gal into consideration, we designed a ^{19}F MRI probe Gd-DFP-Gal for detecting β-gal activity by combining the paramagnetic relaxation enhancement (PRE) based probe design principle that we previously developed[9] with the structures of conventional β-gal probes (Fig. 1). The transverse relaxation time T_2 of the ^{19}F nucleus near Gd^{3+} is expected to be reduced by the PRE from Gd^{3+}, which has seven unpaired electrons in its 4f orbital. Thus, the T_2 of the trifluoromethyl (CF_3) group of Gd-DFP-Gal was expected to be strongly reduced.

Another designed function of Gd-DFP-Gal is the self-immolative property that can be induced by enzymatic cleavage. When Gd-DFP-Gal is hydrolyzed by β-gal, the probe is expected to be automatically converted to the corresponding quinone methide by the successive elimination of the substituent at the benzyl position.[13] Thus, the T_2 of the trifluoromethyl group extends after the β-galactoside bond is cleaved because of the cancellation of the intramolecular PRE. MRI signal intensity (*i.e.*, the peak height of the NMR signal) is proportional to $\exp(-t/T_2)$, where t is the echo time in the spin-echo method. Thus, the T_2 extension leads to an increase in the MRI signal. On the basis of this principle, we expected that the originally quenched ^{19}F MRI signal of Gd-DFP-Gal would emerge upon the enzyme reaction.

Gd-DFP-Gal was synthesized in five steps (Scheme S1, ESI†). Details of the synthetic procedure are described in the Supporting Information.† As we expected, the NMR peak of Gd-DFP-Gal was not observed, although that of the Gd-free probe DFP-Gal was a sharp single peak (Fig. S2, ESI†). Disappearance of the ^{19}F NMR peak of Gd-DFP-Gal indicates that the T_2 was markedly reduced because of the strong intramolecular PRE.

In vitro detection of β-gal activity by ^{19}F NMR and ^{19}F MRI

Because the relaxation times of Gd-DFP-Gal were dramatically reduced, it was expected that the enzymatic degradation of Gd-DFP-Gal would induce the recovery of the disappeared ^{19}F NMR peak. Gd-DFP-Gal was incubated with β-gal at 37 °C in the reaction buffer (pH 7.3) containing 5% D_2O, and the time course of the ^{19}F NMR peak was monitored (Fig. 2a). A single peak appeared at around 16 ppm (internal standard: sodium trifluoroacetate) and increased in a time-dependent manner. As the progress of the enzyme reaction was confirmed by RP-HPLC, the peak of Gd-DFP-Gal disappeared and a new peak appeared (Fig. 2b). The new peak was identified to be 4-hydroxymethyl-3-trifluoromethylphenol (compound **2**) from the retention time. In addition, the ESI-MS of the HPLC peak fraction gave a molecular weight identical to **2** ($m/z = 192$). No other noticeable peaks in the reaction solution HPLC diagram suggest that Gd-DFP-Gal was converted to **2** by β-galactosidase activity with nearly complete efficiency.

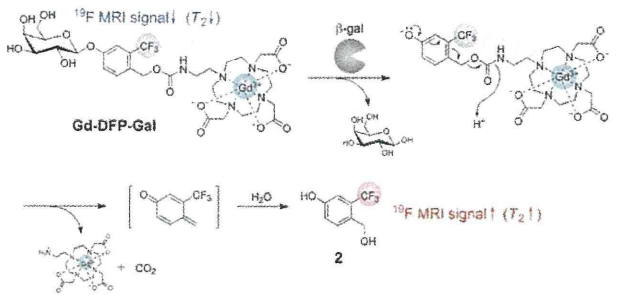

Fig. 1 Structure of Gd-DFP-Gal and the principle for the ^{19}F MRI detection of β-gal activity.

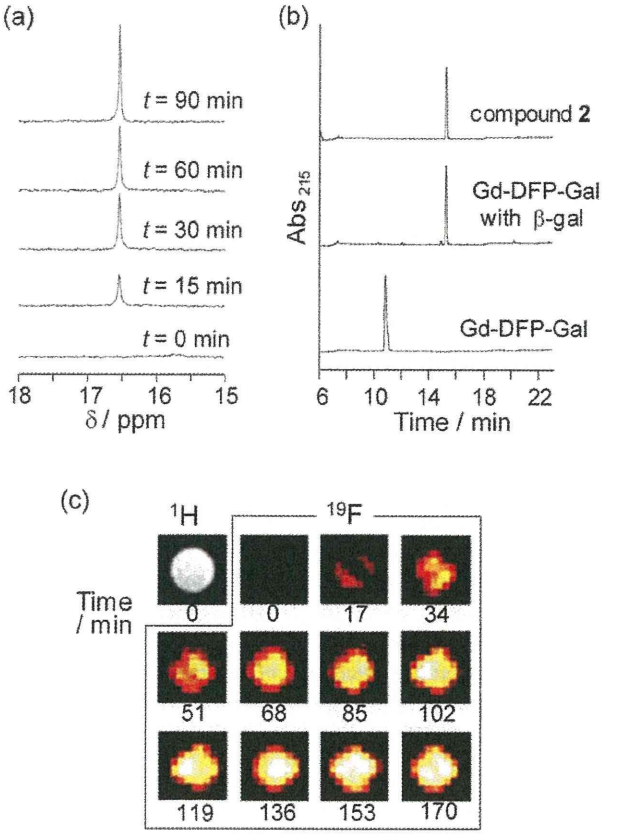

Fig. 2 Detection of β-gal activity by Gd-DFP-Gal. (a) Time-dependent ^{19}F NMR spectral change of Gd-DFP-Gal (1 mM) under incubation with β-gal. Sodium trifluoroacetate was used as the internal standard (0 ppm). (b) Confirmation of the enzymatic cleavage by RP-HPLC (eluent: H_2O–acetonitrile containing 0.1% TFA). (c) Time course of the density-weighted ^{19}F MR phantom images of Gd-DFP-Gal (1 mM) at 37 °C after β-gal was added.

The relaxation times T_1 and T_2 of the reaction sample became 0.306 s and 0.086 s, respectively, after the enzyme reaction. Both of them showed considerable extension compared to those of Gd-DFP-Gal, probably due to the cancellation of the intramolecular PRE from Gd^{3+}. These values are still less than those of the Gd^{3+}-free probe DFP-Gal: 1.293 s for T_1 and 0.271 s for T_2. When the relaxation times of Gd-DFP-Gal were measured at various probe concentrations after the enzymatic cleavage, both T_1 and T_2 extended as the concentration decreased (Fig. S3 and Table S1, ESI†). This concentration dependency of the relaxation times indicates that the intermolecular PRE is effective under the experimental condition even after the enzyme reaction is complete. To confirm the probe specificity, Gd-DFP-gal was incubated with other similar enzymes, α-galactosidase and β-glucuronidase. However, ^{19}F NMR signals of Gd-DFP-gal were not recovered by incubation with such enzymes (Fig. S4, ESI†).

To demonstrate the possibility of further application, ^{19}F MRI detection of β-gal activity was performed using Gd-DFP-Gal. ^{19}F MRI phantom images were measured using an 11.7 T MRI instrument. Gd-DFP-Gal was mixed with *Escherichia coli* β-gal before being poured into a 1-mm-inner radius capillary. The density-weighted MR images were then captured by the fast spin-echo method. As expected from the ^{19}F NMR results, Gd-DFP-Gal showed no ^{19}F MRI signals in the absence of β-gal. After the probe was mixed with β-gal, however, the ^{19}F MRI signals gradually increased in a time-dependent manner (Fig. 2c). Without addition of the enzyme, the MRI image did not show any signals for several hours (data not shown). These results demonstrate that this novel mechanism-based probe Gd-DFP-Gal enables the specific ^{19}F MRI detection of β-gal activity.

^{19}F NMR and ^{19}F MRI detection of β-gal expression in fixed HEK293T cells

Next, the applicability of Gd-DFP-Gal to the detection of intracellular gene expression was confirmed. β-gal was expressed in HEK293T cells, and the cells were fixed with formaldehyde and detergent. Then, Gd-DFP-Gal was incubated with the cells, and β-gal activity in the medium supernatant was analyzed by ^{19}F NMR (Fig. 3a). As a result, incubation of Gd-DFP-Gal only with the cells expressing β-gal induced the clear increase of a single ^{19}F NMR peak (Fig. 3b).

Then, the ^{19}F MRI detection of β-gal gene expression was attempted. HEK293T cells expressing or not expressing β-gal were cultured on 7-mm-diameter glass vessels. After the fixation of the cells, Gd-DFP-Gal (final conc.: 1 mM) was added into the glass vessels, and the cells were incubated at 37 °C for 2 h. The vessels were stacked in an 8 mm NMR tube, as shown in Fig. 3b, and the ^{1}H and ^{19}F MR images were captured. Although both vessels showed indistinguishable signal intensity in ^{1}H MRI (Fig.3c left), only the vessel that included HEK293T cells expressing β-gal showed remarkable ^{19}F MRI signals (Fig. 3c right). These results indicate that Gd-DFP-Gal can specifically detect gene expression in fixed HEK293T cells by means of reporter β-gal activity.

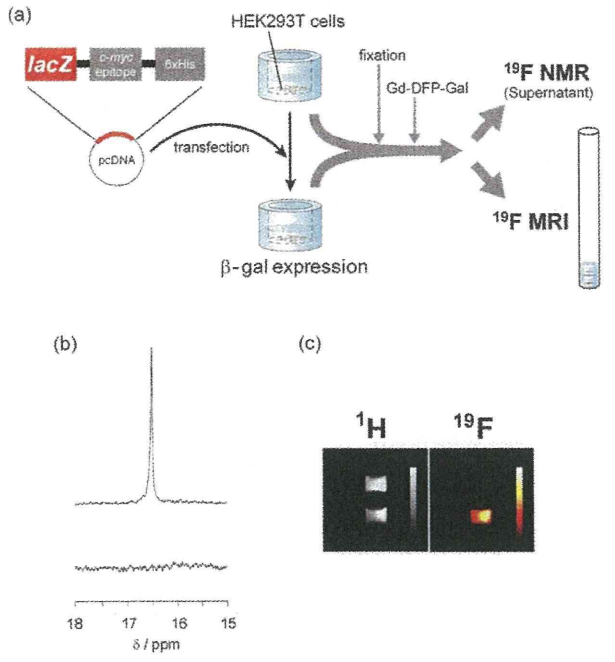

Fig. 3 ^{19}F NMR and ^{19}F MRI detection of gene expression in HEK293T cells. (a) Illustration of the experimental procedures for the ^{19}F NMR and ^{19}F MRI measurements. (b) ^{19}F NMR spectra of the culture medium containing 1 mM Gd-DFP-Gal incubated with fixed cells expressing (top) or not expressing (bottom) β-gal. (c) ^{1}H (left) and ^{19}F (right) MR images of culture vessels containing 1 mM Gd-DFP-Gal fixed cells. Color scale bars were inserted in the images.

Discussion

From the point of probe design strategy, development of Gd-DFP-Gal is an important step forward in molecular imaging studies. Our previous ^{19}F MRI probe that detects protease activity also utilized the cancellation of the intramolecular PRE for signal switching.[9] In these cases, the ^{19}F atoms and the paramagnetic ions were conjugated to each other at the opposite end of the probes (Fig. 4a). The MRI signals were enhanced by enzymatic cleavage of the substrate linker. Although this strategy works for a wide variety of hydrolases such as other proteases, endonucleases and phosphodiesterases, it could not be applied to several hydrolases such as phosphatases that have a substrate-binding pocket covering one end of the substrate. In order to detect these enzyme activities by MRI, we expanded the probe design concept by exploiting a self-immolative reaction, as presented in this study (Fig. 1). We now have the ability to design ^{19}F MRI probes for a broader range of hydrolases by choosing either of the ways illustrated in Fig. 4.

Although imaging of gene expression in fixed cells by using Gd-DFP-Gal, there are two obstacles for future perspective to *in vivo* imaging. One is the membrane permeability of the probes. Since the new probe did not permeate cell membrane, the cells needed to be fixed with formaldehyde for imaging. However, use of cell-penetrating peptides,[14] which enabled the incorporation of proteins into live cells, may dissolve the problem.

The other is the sensitivity. Generally, the sensitivity of ^{19}F MRI probes is worse than ^{1}H MRI probes. This is because ^{1}H MRI visualizes many water molecules around the probe

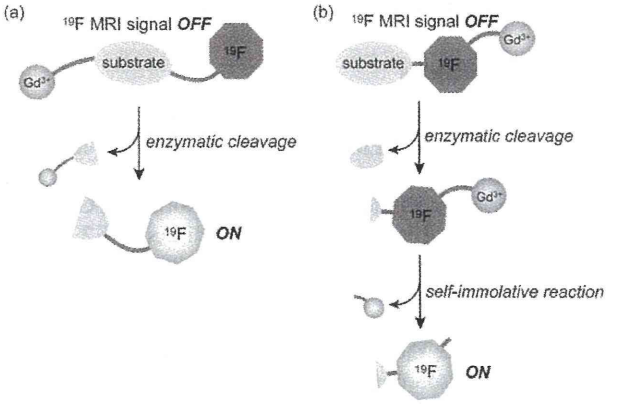

Fig. 4 Two ^{19}F MRI probe design strategies using PRE cancellation by (a) enzymatic cleavage of the substrate linker, and (b) enzyme activity-induced self-immolative reaction.

molecules, although ^{19}F MRI probes give only the probe signals. Concerning the problem, improvement of both probes and instruments will contribute to solve it. About the probe sensitization, we are under the development and would report elsewhere in future.

Conclusions

In summary, we succeeded in the imaging of gene expression in mammalian cells using a novel ^{19}F MRI probe that detects β-gal activity. The probe design concept is based on the MRI signal quenching by PRE. Also, by exploiting a self-immolative organic reaction in the probe design, we could overcome the limitation of our previous probe design, in which the ^{19}F atoms and the paramagnetic ions should be located at the opposite end of the probes. New design strategy will lead to the development of the probes for a wider variety of hydrolases such as phosphatases. Although *in vivo* imaging of gene expression by ^{19}F MRI is still challenging, the further progress of the probe properties will contribute to the solution of the difficult and significant subject.

Experimental section

^{19}F NMR relaxation time measurements

Samples were prepared at 500 μM concentration in 10 mM Tris buffer (pH 7.3) containing 10 mM magnesium chloride and 5% D_2O. The longitudinal relaxation time T_1 was measured by an inversion recovery method and the transverse relaxation time T_2 was measured by the spin-echo method.

Enzyme reaction

Gd-DFP-Gal was dissolved at 500 μM in 10 mM Tris buffer (pH 7.3) containing 10 mM magnesium chloride and 5% D_2O. Samples (500 μL) were incubated with β-gal (5.03 U) at 37 °C for 2 h. The reaction progress was monitored by ^{19}F NMR and RP-HPLC using an octadecyl silane (ODS) column. For the ^{19}F MRI experiment, 1 mM Gd-DFP-Gal was dissolved in 10 mM Tris buffer solution (pH 7.3) containing 10 mM magnesium chloride and 5% D_2O. Samples with or without β-gal (1.2 mU) were filled into glass capillaries (inner diameter: approximately 1 mm; Hischmann Laborgerate). The capillaries were then inserted into an 8 mm NMR tube and the ^{19}F MRI were measured.

Cellular experiments

HEK293T cells were grown at 37 °C in Dulbecco's modified Eagle's medium (DMEM) supplemented with 10% fetal bovine serum (FBS), 100 U mL^{-1} penicillin G, and 100 mg mL^{-1} streptomycin in a humidified atmosphere with 5% CO_2. The cells were plated at 1.2×10^6 cells in 60 mm dishes or 1.2×10^5 cells cm^{-2} on 24-well plates. Next, the cells were transfected with pcDNA™4/TO/*myc*-His/*lacZ*© plasmid using Lipofectamine 2000, and the cells were incubated for 24 h at 37 °C in a CO_2 incubator. After the cells were washed three times with phosphate-buffered solution (PBS), they were incubated with trypsin-EDTA at 37 °C for 5 min under 5% CO_2.

For ^{19}F NMR analysis, the cells were cultured with 1 mM Gd-DFP-Gal for 2 h at 37 °C in the reaction buffer (10 mM Tris-sodium buffer (pH 7.3) and 10 mM magnesium chloride) on 24-well plates. Then, the supernatants were moved into NMR tubes and the ^{19}F NMR spectra were measured.

For ^{19}F MRI analysis, the cells were moved onto 7 mm (outer diameter) glass vessels (Hilgenberg GmbH), and were incubated for 7 h at 37 °C in DMEM with 10% FBS. After the cells were washed three times with PBS, they were incubated with 3.7% formaldehyde for 10 min at room temperature. Then, cells were washed three times with PBS and incubated with 1 mM Gd-DFP-Gal for 2 h at 37 °C in the reaction buffer (Tris-sodium buffer (pH 7.3) and 10 mM magnesium chloride). The vessels were put into an 8 mm NMR tube, and the ^1H and ^{19}F MRI were measured.

Acknowledgements

We thank Dr Tetsuro Kokubo at Yokohama City University for the use of the MRI instrument, and Dr Haruhiko Bito (University of Tokyo), Dr Hiroyuki Okuno (University of Tokyo) and Dr Shin-ichi Muramatsu (Jichi Medical University) for the helpful discussion. This research is supported by Ministry of Education, Culture, Sports, Science and Technology–Japan (Grant No. 21685019 and 20675004), by the Japan Society for the Promotion of Science (JSPS) through its Funding Program for World-Leading Innovative R&D on Science and Technology (FIRST Program), by Ministry of Health, Labour and Welfare–Japan, and by the New Energy and Industrial Technology Development Organization (NEDO) of Japan. S.M. acknowledges the Inamori Foundation.

Notes and references

1 R. Y. Tsien, *Annu. Rev. Biochem.*, 1998, **67**, 509.
2 C. H. Contag and M. H. Bachman, *Annu. Rev. Biomed. Eng.*, 2002, **4**, 235.
3 (*a*) G. P. Nolan, S. Fiering, J.-F. Nicholas and L. A. Herzenberg, *Proc. Natl. Acad. Sci. U. S. A.*, 1988, **85**, 2603; (*b*) I. G. Serebriiskii and E. A. Golemis, *Anal. Biochem.*, 2000, **285**, 1.
4 (*a*) A. Jasanoff, *Trends Neurosci.*, 2005, **28**, 120; (*b*) D. E. Sosnovik and R. Weissleder, *Curr. Opin. Biotechnol.*, 2007, **18**, 4.
5 (*a*) R. Weissleder and M. J. Pittet, *Nature*, 2008, **452**, 580; (*b*) J. L. Major and T. J. Meade, *Acc. Chem. Res.*, 2009, **42**, 893.
6 (*a*) A. Y. Louie, M. M. Hüber, E. T. Ahrens, U. Rothbächer, R. Moats, R. E. Jacobs, S. E. Fraser and T. J. Meade, *Nat. Biotechnol.*, 2000, **18**, 321; (*b*) Y. T. Chang, C. M. Cheng, Y. Z. Su, W. T. Lee, J. S. Hsu, G. C. Liu, T. L. Cheng and Y. M. Wang, *Bioconjugate Chem.*, 2007, **18**, 1716; (*c*) E. L. Que, D. W. Domaille and C. J. Chang, *Chem. Rev.*, 2008, **108**, 1517; (*d*) W. Cui, L. Liu, V. D. Kodibagkar and R. P. Mason, *Magnetic Resonance in Medicine*, 2010, **64**, 65.
7 (*a*) J. Yu, V. D. Kodibagkar, W. Cui and R. P. Mason, *Curr. Med. Chem.*, 2005, **12**, 819; (*b*) C. Belle, C. Beguin, S. Hamman and J.-L. Pierre, *Coord. Chem. Rev.*, 2009, **253**, 963.
8 (*a*) W. Cui, P. Otten, Y. Li, K. S. Koeneman, J. Yu and R. P. Mason, *Magn. Reson. Med.*, 2004, **51**, 616; (*b*) M. Higuchi, N. Iwata, Y. Matsuba, K. Sato, K. Sasamoto and T. C. Saido, *Nat. Neurosci.*, 2005, **8**, 527; (*c*) V. D. Kodibagkar, J. Yu, L. Liu, H. P. Hetherington and R. P. Mason, *Magn. Reson. Imaging*, 2006, **24**, 959; (*d*) K. Tanaka, N. Kitamura, K. Naka and Y. Chujo, *Chem. Commun.*, 2008, 6176; (*e*) P. Porcari, S. Capuani, E. D'Amore, M. Lecce, A. La Bella, F. Fasano, R. Campanella, L. M. Migneco, F. S. Pastore and B. Maraviglia, *Phys. Med. Biol.*, 2008, **53**, 6979; (*f*) K. Tanaka, N. Kitamura, Y. Takahashi and Y. Chujo, *Bioorg. Med. Chem.*, 2009, **17**, 3818; (*g*) Y. Takaoka, T. Sakamoto, S. Tsukiji, M. Narazaki, T. Matsuda, H. Tochio, M. Shirakawa and I. Hamachi, *Nat. Chem.*, 2009, **1**, 557; (*h*) K. Tanabe, H. Harada, M. Narazaki, K. Tanaka, K. Inafuku,

H. Komatsu, T. Ito, H. Yamada, Y. Chujo, T. Matsuda, M. Hiraoka and S. Nishimoto, *J. Am. Chem. Soc.*, 2009, **131**, 15982.
9 (*a*) S. Mizukami, R. Takikawa, F. Sugihara, Y. Hori, H. Tochio, M. Wälchli, M. Shirakawa and K. Kikuchi, *J. Am. Chem. Soc.*, 2008, **130**, 794; (*b*) S. Mizukami, R. Takikawa, F. Sugihara, M. Shirakawa and K. Kikuchi, *Angew. Chem., Int. Ed.*, 2009, **48**, 3641.
10 L. Helm, *Prog. Nucl. Magn. Reson. Spectrosc.*, 2006, **49**, 45.
11 C. V. Hall, P. E. Jacob, G. M. Ringold and F. Lee, *J. Mol. Appl. Genet.*, 1983, **2**, 101.
12 (*a*) J. P. Horwitz, J. Chua, R. J. Curby, A. J. Tomson, M. A. DaRooge, B. E. Fisher, J. Mauricio and I. Klundt, *J. Med. Chem.*, 1964, **7**, 574; (*b*) A. B. Pardee, F. Jacob and J. Monod, *J. Mol. Biol.*, 1959, **1**, 165.
13 (*a*) D. Shabat, R. J. Amir, A. Gopin, N. Pessah, M. Shamis and W.-M. Dai, *Chem.–Eur. J.*, 2004, **10**, 2626; (*b*) J. A. Duimstra, F. J. Femia and T. J. Meade, *J. Am. Chem. Soc.*, 2005, **127**, 12847; (*c*) T. Komatsu, K. Kikuchi, H. Takakusa, K. Hanaoka, T. Ueno, M. Kamiya, Y. Urano and T. Nagano, *J. Am. Chem. Soc.*, 2006, **128**, 15946; (*d*) N.-H. Ho, R. Weissleder and C.-H. Tung, *ChemBioChem*, 2007, **8**, 560.
14 E. Vives, J. Schmidt and A. Pelegrin, *Biochim. Biophys. Acta*, 2008, **1786**, 126.

CHEMISTRY
A EUROPEAN JOURNAL

DOI: 10.1002/chem.201100973

Intracellular Protein Labeling with Prodrug-Like Probes Using a Mutant β-Lactamase Tag

Shuji Watanabe,[a] Shin Mizukami,[a, b] Yuri Akimoto,[a] Yuichiro Hori,[a] and Kazuya Kikuchi*[a, b]

Abstract: Intracellular protein labeling with small molecular probes that do not require a washing step for the removal of excess probe is greatly desired for real-time investigation of protein dynamics in living cells. Successful labeling of proteins on the cell membrane has been performed using mutant β-lactamase tag (BL-tag) technology. In the present study, intracellular protein labeling with novel cell membrane permeable probes based on β-lactam prodrugs is described. The prodrug-based probes quickly permeated the plasma membranes of living mammalian cells, and efficiently labeled intracellular proteins at low probe concentrations. Because these cell-permeable probes were activated only inside cells, simultaneous discriminative labeling of intracellular and cell surface BL-tag fusion proteins was attained by using cell-permeable and impermeable probes. Thus, this technology enables adequate discrimination of the location of proteins labeled with the same protein tag, in conjunction with different color probes, by dual-color fluorescence. Moreover, the combination of BL-tag technology and the prodrug-based probes enabled the labeling of target proteins without requiring a washing step, owing to the efficient entry of probes into cells and the fast covalent labeling achieved with BL-tag technology after bioactivation. This prodrug-based probe design strategy for BL-tags provides a simple experimental procedure with application to cellular studies with the additional advantage of reduced stress to living cells.

Keywords: fluorescent probes · microscopy · prodrugs · protein labeling · β-lactamase

Introduction

The specific labeling of proteins using small molecule probes has attracted much attention for the investigation of protein structure, function, localization, and protein–protein interactions.[1] The modification of target proteins with small molecules such as near-infrared fluorophores, biofunctional molecules such as biotin, and magnetic resonance imaging (MRI) agents enables a wider range of functional studies than those achieved with fluorescent proteins (FPs). Various labeling methods have been developed based on enzyme-catalyzed modification,[2] specific chelation of fluorescent ligands to short peptides,[3] and self-labeling protein tags.[4] Several reported labeling methods however, are restricted to labeling of cell surface proteins because of the cell impermeability of labeling probes or the presence of endogenous counterparts within cells.[5]

We recently described a novel method for the highly specific labeling of proteins by exploiting a mutant of 29 kDa TEM-1 β-lactamase.[6] TEM-1 efficiently hydrolyzes β-lactam derivatives and affords the corresponding hydrolysates.[7] During enzymatic hydrolysis by a wild-type TEM-1, Ser70 in the active site of the enzyme attacks the β-lactam carbonyl carbon and the nucleophilic substitution produces the acyl–enzyme intermediate. Subsequently, the acyl–enzyme intermediate is hydrolyzed by water molecules activated by a proximate carboxylate anion of Glu166. Prior studies in the E166N mutant showed that the acyl–enzyme intermediates remain stable. The labeling system involves covalent modification of the mutant TEM-1 (BL-tag) with the fluorescent β-lactam derivatives (Scheme 1a). Because these β-lactam derivatives have a carboxylate within their structure, they intrinsically show reduced transmembrane permeability.

For the intracellular application of the BL-tag technology, we focused on the prodrugs of β-lactam antibiotics that are based on the modification of carboxylic acids to noncharged ester derivatives. Prodrugs are commonly designed to improve oral bioavailability compared with the parent drugs.[8] The absorption, stability, and toxicity of the prodrugs have been rigorously investigated through rational molecular design. Although the esterified β-lactam prodrugs are inactive to β-lactamases,[9] the ester group of the prodrug is

[a] S. Watanabe, Dr. S. Mizukami, Y. Akimoto, Dr. Y. Hori, Prof. Dr. K. Kikuchi
Division of Advanced Science and Biotechnology
Graduate School of Engineering, Osaka University
2–1 Yamadaoka, Suita, Osaka 565-0871 (Japan)
Fax: (+81)6-6879-7875
E-mail: kkikuchi@mls.eng.osaka-u.ac.jp

[b] Dr. S. Mizukami, Prof. Dr. K. Kikuchi
Immunology Frontier Research Center (IFReC), Osaka University,
3–1 Yamadaoka, Suita, Osaka 565-0871 (Japan)

Supporting information for this article is available on the WWW under http://dx.doi.org/10.1002/chem.201100973.

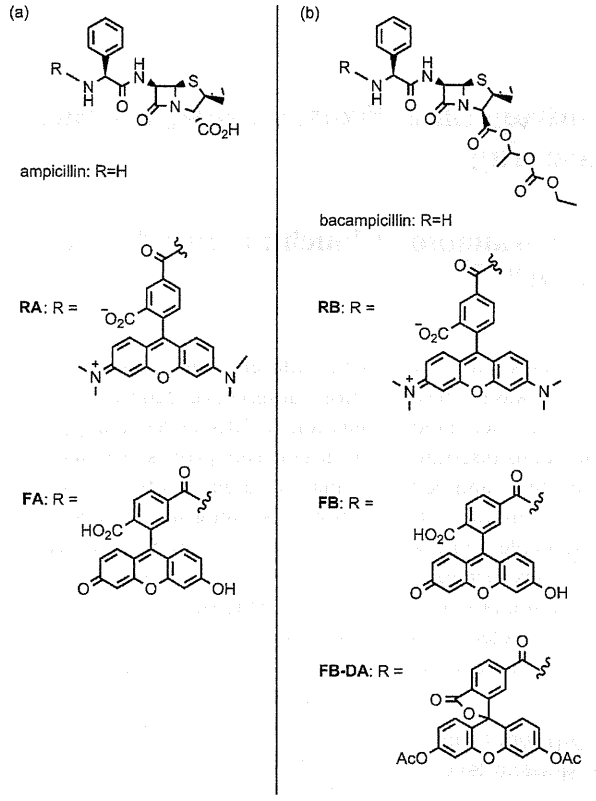

Scheme 1. Structures of a) reported ampicillin-based probes (**RA** and **FA**) and b) newly synthesized bacampicillin-based probes (**RB**, **FB**, and **FB-DA**) for BL-tag.

quickly converted into a carboxylate by the activities of intracellular esterases, which results in the accumulation of active β-lactams in cells. Thus, the labeling properties of probes can be made dependent on location by exploiting the structure of the prodrug.

Although the intracellular application of target protein labeling has been reported previously,[3,4] washing of unreacted probes, which was a necessary step in prior work, limits the robustness of the method because it is nearly impossible to completely wash out the probes in the cytoplasm. We assumed that this drawback was due to both the low efficiency of the membrane permeation and the low efficiency of the reaction with the target protein. The BL-tag technology enables simple and wide variations of probe design. In addition, BL-tag technology results in high reaction efficiency due to the use of mutated proteins that do not limit substrate entrance. Therefore, efficient delivery of the probe to the intracellular target protein allows its specific labeling without the requirement for a washing step. On the basis of these requirements, we investigated the development of probes designed for effective transport into cells using our BL-tag technology.

The present study describes a novel design strategy for cell-permeable probes for BL-tag technology based on the use of a clinical β-lactam prodrug. These bioactivation-process-based probes enabled the discrimination between same tag proteins in different locations using dual-color fluorescence. Moreover, specific labeling of intracellular target proteins without the required washing of excess probe was achieved based on the fast permeation and accumulation of labeling probes.

Results and Discussion

Design and synthesis of cell-permeable probes based on β-lactam prodrug structures: Three representative ampicillin esters (bacampicillin, pivampicillin, and talampicillin) have been well studied for their bioavailability among the clinical prodrugs of ampicillin (Scheme 1).[10] The carboxy groups of these prodrugs are converted into noncharged and lipophilic ester groups to increase the bioavailability of ampicillin. We chose bacampicillin as the core structure for the cell-permeable labeling probes because among the studied prodrugs, bacampicillin shows the best absorption by the body and is stable at neutral pH,[11] as well as being industrially available.[12] Although bacampicillin itself exhibits low antibacterial activity, once it is transformed into ampicillin by the bioactivation process, it shows high antibacterial activity (Scheme 1).[13]

The bacampicillin-based probes **RB**, **FB**, and **FB-DA** (Scheme 1b) were designed and synthesized as described in the Supporting Information (see Scheme S1). **RB** and **FB**, which are fluorophore-attached bacampicillin derivatives, were synthesized in one step by a condensation reaction of bacampicillin hydrochloride with the activated ester of the corresponding fluorophores. **FB-DA** is the diacetylated counterpart of **FB** designed for increased cell permeability. Absorption and emission spectra of the synthesized probes are shown in Figure S1 in the Supporting Information section. The fluorescence quantum yields of **RB** and **FB** were 0.50 and 0.55, respectively. Therefore, the esterification of the carboxy group of ampicillin has almost no effect on the spectroscopic properties of the conjugated fluorophore. Although **FB-DA** showed no fluorescence, this is a known characteristic of diacetylated fluorescein derivatives.[14]

The in vitro enzymatic conversion of the bacampicillin moiety to the ampicillin moiety of the synthesized probes was confirmed. HPLC and ESI-TOF MS analyses of the reaction mixture of **RB** with an esterase demonstrated the complete conversion of **RB** into **RA** (Figure S2 in Supporting Information), which specifically labels BL-tag fusion proteins.[6b] The addition of an esterase shifted the retention time of **RB**, resulting in a new peak with the same *m/z* value ($[M+H]^+$: 762.3) as that of **RA** in the MS analysis.

Specific labeling of intracellular BL-tag fusion proteins with bacampicillin-based probes: The newly synthesized probes were used for intracellular protein labeling using BL-tag technology (Scheme 2). In *E. coli*, the unmodified coding region of β-lactamase contains a signal peptide sequence for secretion into the periplasm.[15] To generate an intracellular

